Evidence for increased hominid diversity in the Early to Middle Pleistocene of Indonesia

Clément Zanolli, Ottmar Kullmer, Jay Kelley, Anne-Marie Bacon, Fabrice Demeter, Jean Dumoncel, Luca Fiorenza, Frederick Grine, Jean-Jacques Hublin, Nguyen Anh Tuan, et al.

Evidence for increased hominid diversity in the Early-Middle Pleistocene of Indonesia

Clément Zanolli[1,2*], Ottmar Kullmer[3,4], Jay Kelley[5,6,7], Anne-Marie Bacon[8], Fabrice Demeter[9,10], Jean Dumoncel[1], Luca Fiorenza[11,12], Frederick E. Grine[13], Jean-Jacques Hublin[14], Nguyen Anh Tuan[15], Nguyen Thi Mai Huong[15], Lei Pan[16,17], Burkhard Schillinger[18], Friedemann Schrenk[3,4], Matthew M. Skinner[14,19], Xueping Ji[20,21] & Roberto Macchiarelli[22,23]

[1]Laboratoire AMIS, UMR 5288 CNRS, Université Toulouse III Paul Sabatier, Toulouse, France. [2]Laboratoire PACEA, UMR 5199 CNRS, Université de Bordeaux, France. [3]Department of Palaeoanthropology, Senckenberg Research Institute and Natural History Museum Frankfurt, Frankfurt a.M., Germany. [4]Department of Paleobiology and Environment, Institute of Ecology, Evolution, and Diversity, Goethe University Frankfurt, Germany. [5]Institute of Human Origins and School of Human Evolution and Social Change, Arizona State University, Tempe, USA. [6]Department of Paleobiology, National Museum of Natural History, Smithsonian Institution, Washington D.C., USA. [7]Department of Human Evolutionary Biology, Harvard University, Cambridge, USA. [8]Laboratoire AMIS, UMR 5288 CNRS, Université Paris Descartes, Faculté de chirurgie dentaire, Montrouge, France. [9]UMR 7206 CNRS, Muséum National d'Histoire Naturelle, Paris, France. [10]Center for GeoGenetics, Copenhagen, Denmark. [11]Department of Anatomy and Developmental Biology, Monash University, Melbourne, Australia. [12]Earth Sciences, University of New England, Armidale, Australia. [13]Department of Anthropology and Department of Anatomical Sciences, Stony Brook University, Stony Brook, USA. [14]Department of Human Evolution, Max Planck Institute for Evolutionary Anthropology, Leipzig, Germany. [15]Anthropological and Palaeoenvironmental Department, The Institute of Archaeology, Hanoi, Vietnam. [16]Key Laboratory of Vertebrate Evolution and Human Origins, Institute of Vertebrate Paleontology and Paleoanthropology, Chinese Academy of Sciences, Beijing, China. [17]State Key Laboratory of Palaeobiology and Stratigraphy, Nanjing Institute of Geology and Palaeontology, Chinese Academy of Sciences, Nanjing, China [18]Heinz Maier-Leibnitz Center (FRM-II), Technische Universität München, Garching, Germany. [19]School of Anthropology and Conservation, University of Kent, Canterbury, UK. [20]Department of Paleoanthropology, Yunnan Institute of Cultural Relics and Archaeology, Kunming 650118, China. [21]School of Resource Environment and Earth Science, Yunnan University, Kunming, China. [22]UMR 7194 CNRS, Muséum National d'Histoire Naturelle, Paris, France. [23]Unité de Formation Géosciences, Université de Poitiers, France.

Since the first discovery of *Pithecanthropus* (*Homo*) *erectus* by E. Dubois at Trinil in 1891, over 200 hominid dentognathic remains have been collected from the Early-Middle Pleistocene deposits of Java, Indonesia, forming the largest palaeoanthropological collection in Southeast Asia. Most of these fossils are currently attributed to *H. erectus*. However, because of the substantial morphological and metric variation in the Indonesian assemblage, some robust specimens, such as the partial mandibles Sangiran 5 and Sangiran 6a, were formerly variably allocated to other taxa (*Meganthropus palaeojavanicus*, *Pithecanthropus dubius*, *Pongo* sp.). To resolve the taxonomic uncertainty surrounding these and other contentious Indonesian hominid specimens, we used Occlusal Fingerprint Analysis to reconstruct their chewing kinematics, and also used various morphometric approaches based on microtomography to examine internal dental structures. Our results confirm the presence of *Meganthropus* as a Pleistocene Indonesian hominid distinct from *Pongo*, *Gigantopithecus* and *Homo*, and further reveal that

Eugene Dubois' *Homo erectus* paratype molars from 1891 are not hominin (human lineage), but instead are more likely to belong to *Meganthropus*.

During the Quaternary, episodes of glacial eustasy combined with tectonic uplift and volcaniclastic deposition periodically altered the palaeobiogeography of the Sunda region. These physical and resultant environmental changes facilitated or inhibited intermittent faunal exchanges with the Asian mainland[1] and influenced the evolutionary dynamics of the local faunas, including hominids[2]. The presence of hominids (great apes and humans) in Southeast Asia during the Early and Middle Pleistocene is well documented in the fossil record, with at least three firmly established genera: *Gigantopithecus*, *Pongo* and *Homo*[3-6]. The existence of a putative "mystery ape" has also been evoked[7]. Due to the implied vicariance and relict survivorship accompanying these geomorphological events, the appraisal of palaeobiodiversity at a regional scale is difficult. The presence of *Homo* in insular Southeast Asia since the Early Pleistocene has been amply documented by cranial, dental and postcranial remains[3]. Conversely, apart from four isolated teeth recently discovered in Peninsular Malaysia[8], only a few dental specimens representing *Pongo* sp. have been reported from the Early and Middle Pleistocene deposits of Indonesia[9]. Because of the convergence in molar crown size and overall morphology between fossil *Homo* and *Pongo*, the taxonomic diagnosis of many Asian Early Pleistocene hominid dentognathic specimens has been debated for over a century, especially concerning isolated teeth and occlusally worn specimens[10,11] (Supplementary Figure 1 and Supplementary Material). The resulting taxonomic confusion has affected the historical debate on the evolution of the genus *Homo* in Southeast Asia and, more generally, the assessment of Pleistocene hominid palaeobiodiversity[7].

Using three-dimensional virtual imaging, we reassess the taxonomic assignment of two isolated maxillary molars from Trinil (Trinil 11620 and Trinil 11621)[10,11], paratypes of *H. erectus*[12], and of the partial mandibles Sangiran 5, the holotype of *Pithecanthropus dubius*[13], and Sangiran 6a, the holotype of *Meganthropus paleojavanicus*[14,15], all currently considered to be *H. erectus*[16-18]. We also re-examine the mandibular specimen Arjuna 9, regarded as a robust *H. erectus* similar to Sangiran 6a[19], and seven isolated upper and lower permanent molar crowns from the Early-Middle Pleistocene Sangiran Dome formations (FS-77, SMF-8855, SMF-8864, SMF-8865, SMF-8879, SMF-8898 and SMF-10055), provisionally labelled as *Pongo* sp., but whose taxonomic identity remains problematic (Figure 1, Supplementary Figure 2 and Supplementary Material). The analyses and/or examined features include Occlusal Fingerprint Analysis, enamel distribution and relative enamel thickness, crown-root surface area proportions, enamel-dentine junction topography, and pulp chamber morphology. We compare the results from this Indonesian assemblage with similar data from extant and fossil *Homo* and *Pongo*, as well as the fossil hominids *Sivapithecus* (Late Miocene, South Asia),

Lufengpithecus (Late Miocene, southern China), and *Gigantopithecus* (Pleistocene, China and Southeast Asia)[20] (Supplementary Tables 1-4).

Results

One important distinction between humans and non-human apes concerns their dietary ecology and feeding behaviours, reflected in their masticatory apparatus by different morphological adaptations and structural characteristics[21,22]. Occlusal Fingerprint Analysis[23] of crown wear patterns reveals that all robust Indonesian hominid molars suitable for this investigation (9 of 13) exhibit an ape-like functional macrowear pattern that differs significantly (p<0.05) from that of extant and extinct hominin samples, including Javanese *H. erectus* (Figure 2 and Supplementary Table 5). This pattern is characterised by a high dominance of power stroke Phase II over Phase I, evidenced by enlarged Phase II wear facets (Supplementary Table 6). In contrast, humans and extinct hominins, including Chinese and Indonesian *H. erectus*, display proportionately larger buccal Phase I wear facets, indicative of distinct masticatory behaviour (Figure 2).

Patterns of enamel distribution are sensitive indicators of dietary adaptations and taxonomic affinities in anthropoids[22]. Morphometric cartographies distinguish between hominin and ape patterns: in the former, the thickest enamel is deposited on the "functional cusps" rather than on the "guiding" cusps[22], while in apes, and notably in *Pongo*, it lies at the periphery of the occlusal basin[24-26]. Our analyses reveal that all but one of the modestly worn hominid molars from Java (n=8) show an ape pattern. The maxillary molar Trinil 11620 displays even relatively thicker enamel at the periphery of the occlusal basin than is typically found in *Pongo*, more closely approximating the Miocene apes *Sivapithecus* and *Lufengpithecus* (Figure 3). Conversely, the lower molar specimen SMF-8865 closely resembles the condition characterising African and Indonesian *H. erectus*, showing the thickest enamel localized on the buccal cusps, while Arjuna 9, FS-77, SMF8855, SMF-8864 and SMF-8879 have the thickest enamel distributed along the marginal ridges around the occlusal basin. Crown tissue proportions, including the commonly used Relative Enamel Thickness index[24,26,27], overlap across all extinct and extant samples and do not discriminate the Javanese robust specimens (Supplementary Figure 3 and Supplementary Tables 7-8).

Crown-root surface area proportions have also been demonstrated to show a strong phylogenetic signal, independent of feeding adaptions in tooth morphology[28]. Both upper molars from Trinil and the lower post-canine teeth of Sangiran 6a and Arjuna 9 exhibit proportionally large root surfaces compared to the lateral (non-occlusal) crown area, resembling pongines and *Lufengpithecus* and differing substantially from *Homo* (Figure 4, Supplementary Figure 4 and Supplementary Table 9).

The topography of the enamel-dentine junction (EDJ), which reliably distinguishes fossil and extant hominid taxa[24,26,29], approximates the inner enamel epithelium of the developing tooth and

provides useful information about taxon-specific processes underlying crown growth[29]. Six of the Javanese lower molars show a cingulum-like, mesiodistally extended buccal protostylid at the EDJ, which is distinct from the morphology commonly found in *Homo* and *Pongo* but similar to the condition expressed by the Miocene Chinese ape *Lufengpithecus* (Supplementary Figure 5; see also Supplementary Figure 6 for the lower P4 EDJ morphology). The specimen SMF-8865 does not show the same coarse wrinkling pattern at the EDJ as the other robust Indonesian hominids, or the dense crenulation pattern typical of *Pongo*, but rather resembles the *H. erectus* condition (Supplementary Figure 5).

We also performed geometric morphometric (GM) analyses of the molar EDJ to compare the Indonesian fossil specimens to an assemblage of fossil and extant hominids (Figure 5). The results show statistical discrimination between *Pongo* and *Homo* and unambiguously classify the robust Javanese specimens as non-human apes, again with the exception of SMF-8865 (Supplementary Table 10). Indeed, except for the latter specimen, the EDJ shape of this Javanese sample of robust teeth is distinguished from *Homo* and overlaps those of *Pongo* and *Lufengpithecus*, even if some specimens like the holotype of *Meganthropus*[14,15], Sangiran 6a, are outside the variation of *Pongo* (Figure 5, Supplementary Figure 7). As in fossil *Pongo*[24], *Gigantopithecus*[24], *Sivapithecus* and *Lufengpithecus*, the EDJ of these teeth consistently exhibits a low topography with higher mesial than distal dentine horns. Interestingly, comparable results are obtained when the same analysis is performed on the lower P4 of Sangiran 6a (Supplementary Figures 8-9 and Supplementary Table 11). Conversely, in *Homo*[26,29] and in SMF-8865 as well, the EDJ typically shows higher relief, with dentine horns of sub-equal height and more distally-set buccal cusps (Figure 5). In light of this, it is noteworthy that a pongine-like endostructural signature (but different from that typical of *Pongo*) was recently identified in an isolated deciduous mandibular molar from the Early Pleistocene of Sangiran that was originally labelled as *Meganthropus*[14], but later allocated to early *Homo* (rev. in ref. 26).

While the taxonomic significance of the EDJ is supported by previous studies[29], that of pulp chamber shape has not been systematically evaluated. However, marked morphological differences are notable in the height, thickness and shape of the pulp chamber between fossil and extant hominid taxa (Supplementary Figures 10-11). Accordingly, we performed a preliminarily GM analysis limited to the four extant hominid genera. Our results demonstrate that *Homo* and *Pongo* are statistically distinguished by pulp chamber morphology (Supplementary Material and Supplementary Figure 12). Based on these results, three-dimensional landmark-based analyses of the shape of the pulp chamber (not possible for SMF-8865) were thus extended to the fossil specimens. Similar to the analyses of the EDJ, they clearly discriminate the robust Javanese specimens from *Homo* (Supplementary Table 10). However, in contrast to the results of EDJ shape, the shape of the pulp chamber also distinguishes most of the fossil specimens forming the Javanese assemblage from *Pongo* (except for SMF-8879)

and approximates *Lufengpithecus* (Figure 5 and Supplementary Figure 13).

When only non-hominin taxa are considered in the GM analyses of the EDJ and pulp chamber, the robust Indonesian molars are generally distinguished from *Pongo* (except for SMF-8879, which falls close to or within the *Pongo* range of variation) and approximate the Miocene representatives, especially *Lufengpithecus* (Figure 6 and Supplementary Figures 14-15).

Discussion

Previous attempts to sort the Indonesian hominid dentognathic remains into morphs primarily based on their external morphology provided different, sometimes contradictory, results[7,18,19,30]. This is because the fossil assemblage shows variable preservation conditions and most dental remains are affected by extensive occlusal wear (Supplementary Figure 1). Based on multiple aspects of dental morphology, our re-analysis of this long-controversial sample of robust Pleistocene dentognathic specimens from Java demonstrates that, with the exception of the isolated crown SMF-8865, which we attribute to *H. erectus*, all the specimens investigated here most likely represent non-hominin species. Moreover, Trinil 11620, Trinil 11621, Sangiran 5, Sangiran 6a, Arjuna 9, FS-77 and SMF-8864 are dentally distinct from *Pongo* and represent a third ape lineage in addition to *Pongo* and *Gigantopithecus* that survived beyond the Miocene in South-eastern Asia. We propose to allocate this material to the resurrected species *Meganthropus palaeojavanicus* von Koenigswald, 1950[14,15], but as a non-hominin. The holotype is Sangiran 6a and the other specimens are paratypes. Consequently, *Pithecanthropus dubius*[15] becomes a junior synonym of *Meganthropus palaeojavanicus*.

Unlike most apes, Sangiran 6a and Sangiran 9[14-17] lack the canine/P3 honing complex and the P3 is non-sectorial, being more similar to the P4 with reduced crown height, a relatively prominent metaconid (thus being clearly bicuspid) and a more buccolingually oriented crown major axis. In all these features, *Meganthropus* is similar to Plio-Pleistocene hominins, which might argue for *Meganthropus* being a hominin rather than a non-hominin hominid as we conclude from our analysis of internal dental structure. However, there are other fossil apes in which the P3 is non-sectorial and converges on a hominin-like morphology, most strikingly among megadont species that have undergone marked canine reduction, such as the Late Miocene *Indopithecus*[31], and especially the Pleistocene *Gigantopithecus*[6,32], in which the P3 is typically bicuspid. A relatively low-crowned and more transversely oriented P3 associated with some degree of canine reduction (at least with respect to its cervical dimensions) also characterises the Late Miocene megadont *Ouranopithecus*[33]. While having a sectorial P3, *Lufengpithecus* also shows strong expression of the metaconid, in some cases bordering on a bicuspid morphology[34].

Concerning Trinil 11620, this tooth was among those in another recent attempt to sort out the identities of Pleistocene dental remains, mostly from China but including several teeth from Southeast

Asia as well[11]. Other than 2D enamel thickness and EDJ topography, that study examined different aspects of dental morphology than those examined here, and, with the exception of Trinil 11620, on an entirely different sample. While Trinil 11620 is identified *a priori* as a hominin in that study and another previous study[11,35], this is based on a prior analysis[10] to decide only whether it should be assigned to *Homo* or *Pongo*, without considering the possible presence of an additional Pleistocene ape lineage in Southeast Asia in addition to *Pongo* and *Gigantopithecus*. Also, no results or conclusions are reported for it other than a long-period (Retzius) developmental line periodicity of either 6 or 7[10]. These values are well below the reported range of periodicities for fossil or extant *Pongo* and a value of 6 would be an unusually low value for fossil or extant *Homo*[11,35,36]. While *Gigantopithecus* and *Sivapithecus* typically show values of 8-11 days[11,37], we note that in a small sample of *Lufengpithecus*, the Retzius line periodicity is 7-9 days[38]. Although we did not examine long-period line periodicity, and there is substantial variation in long-period line periodicities in hominid taxa[35,36], the low value for Trinil 11620 could perhaps be considered as additional support for the assignment of this tooth to *Meganthropus.*

In keeping with its prior definition, *Meganthropus* is distinguished from *Homo* by having absolutely large teeth[14,15], a mandibular corpus with a thick and rounded inferior border, a large extramolar sulcus and strong lateral prominence[15-17], molarised premolars, and low molar crowns with coarse wrinkling converging toward the centre of the occlusal surface[14,15]. Our results demonstrate that *Meganthropus* is further distinguished from *Homo* by an ape-like molar occlusal macrowear pattern, peripherally-distributed thicker molar enamel, a low crowned EDJ with relatively short dentine horns, a particularly slender pulp shape with high horns, and lower crown/root surface area proportions. It further differs from penecontemporaneous *H. erectus* by the presence of a cingulum-like protostylid in both the enamel and the underlying EDJ. This feature is commonly found in *Australopithecus* and *Paranthropus*, but *Meganthropus* differs from these two hominins by its ape-like occlusal wear pattern (Supplementary Figure 16), thicker peripheral enamel (whereas thicker enamel is found at the cusp tip in australopiths[39]), the lower EDJ topography, and more slender pulp chamber with vertically elongated pulp horns (Supplementary Figure 17). As a further consequence of recognising *Meganthropus* as non-hominin, certain features commonly regarded as characteristic of hominins, such as the loss of the canine/P3 honing complex, lack of a marked mandibular simian shelf, moderately mesiodistally elongated premolars with a double root and premolar/molar size proportions[12,14-17], more likely represent homoplastic traits in *Meganthropus*. From our results, it is also evident that, aside from marked differences in mandibular morphology and proportions, *Meganthropus* differs from *Pongo* by having laterally-positioned molar dentine horns, a slender pulp chamber, and a cingulum-like expression of the protostylid (Figure 6 and Supplementary Figures 5 and 10). *Meganthropus* is also clearly distinct from *Gigantopithecus*, the latter displaying higher-

crowned and narrower molars with low bulbous cusps and rounded crests, a large cuspule formed by a lobe between the protoconid and metaconid giving the lower molars a distinctive cusp pattern comprised of two pairs of main cusps arranged peripherally, a line of smaller midline cusps that includes the talonid cuspule and the hypoconulid, the lack or faint expression of the protostylid, strong buccolingual mid-crown waisting[6], thicker occlusal enamel, and higher EDJ topography[24] (for a detailed differential diagnosis of *Meganthropus*, see Supplementary Material section 3, Supplementary Figure 18 and Supplementary Table 12).

We provisionally assign SMF-8879 to *Pongo* sp. Future analyses should clarify the taxonomic status of the specimens SMF-8855, SMF-8898 and SMF-10055, currently regarded as pongines, but which also share some features with the Asian Miocene apes, as well as other specimens from Early Pleistocene Java whose status continues to be debated (e.g., Sangiran 8, Sangiran 9, Sangiran 27)[16,17].

Across most of Eurasia, apes became extinct prior to the end of the Miocene. They survived into the Pleistocene only in South-eastern Asia, represented by *Gigantopithecus* and *Pongo*, both known from southern-most China into Southeast Asia[5,40]. To these can be added *Meganthropus* from Java, formerly suggested to be an ape by some[12,14,15] but only confidently demonstrated to be so by the comparative analyses presented here. As demonstrated by paleobotanical, paleontological and geochemical proxies[2,41-43], the Early to Middle Pleistocene palaeoenvironments of Sangiran and Trinil included a variety of mixed and temporally shifting habitats, ranging from open woodland areas to dense forests capable of supporting the presence of multiple large-bodied hominid species in addition to at least two arboreal monkeys, *Macaca fascicularis* and *Trachypithecus cristatus*[2]. Of the other apes present during the late Miocene in South and Southeast Asia - *Sivapithecus*, *Khoratpithecus*, and *Lufengpithecus* - *Meganthropus* appears to be dentally most similar to the last, evidenced by the presence in both of low-cusped and wrinkled molar crowns[21,44,45] with a squat EDJ, an extended protostylid and a slender pulp chamber (Figure 5, Supplementary Figures 5 and 10). In contrast, *Sivapithecus* and *Khoratpithecus* have higher, more bunodont molars with marked mid-crown buccolingual constriction[21,22] and *Sivapithecus* has proportionally higher dentine horns (Figure 5). In sum, when combining evidence from the occlusal wear pattern, internal tooth structure, and aspects related to dental development[10], *Meganthropus* shows greatest affinity to *Lufengpithecus*, and we hypothesize that these taxa are phylogenetically closely related. Substantiating this will require fuller knowledge than currently available of character polarity and homology versus homoplasy in features of tooth internal structure and dental development as a whole.

Conclusion

During the Early-Middle Pleistocene, at least three and perhaps four hominid genera inhabited what is now Indonesia: *Homo*, *Pongo* and *Meganthropus*, with the possible presence of *Gigantopithecus*[40].

This is a higher level of diversity than previously recognised and, with the newly resurrected genus *Meganthropus* now recognized as an ape, is particularly noteworthy for the late survival of two to three large ape lineages. Whether related to the expansion of *H. erectus*, palaeoenvironmental changes, competition with *Pongo* or *Gigantopithecus*, or some combination of these factors, *Meganthropus* did not persist beyond the Middle Pleistocene, leaving only three species of the genus *Pongo* (*P. pygmaeus*, *P. abelii* and *P. tapanuliensis*) subsisting today in remote and protected Indonesian localities[46].

Methods

X-ray and neutron microtomography. Except for the Trinil molars and Sangiran 5 (see below), all Javanese hominid specimens studied here (Sangiran 6a, Arjuna 9, FS-77, SMF-8855, SMF-8864, SMF-8865, SMF-8879, SMF-8898 and SMF-10055) were scanned using the X-ray microfocus sources (X-µCT) at: the Helmholtz-Zentrum Berlin (equipment CONRAD II instrument), the Department of Human Evolution of the Max Plank Institute of Leipzig (equipment BIR ACTIS 225/300), the University of Poitiers (equipment X8050-16 Viscom AG), and the Seckenberg Research Institute (Phoenix Nanotom s 180). Acquisitions were performed according to the following parameters: 100-160 kV, 0.11-90 µA, 0.14-0.36° of angular step. The final volumes were reconstructed with voxel sizes ranging from 20.8 to 40.7 µm. The two Trinil molars (11620 and 11621) were scanned by SR-µCT on beamline ID 19 of the European Synchrotron Radiation Facility at Grenoble using absorption mode with an isotropic voxel size of 31.12 μm^3 at an energy of 60 keV[10]. The dataset of 632 images is available in 8 bits .tif format at the ESRF Paleontological Database (http://paleo.esrf.eu). The X-µCT acquisitions of the comparative fossil and extant hominid specimens were performed using various equipment with the following parameters: 95-145 kV, 0.04-0.40 µA, 0.17-0.36° of angular step. The final volumes were reconstructed with voxel sizes ranging from 8.3 to 60.0 µm.

The specimens Sangiran 5 and Sangiran 6a were scanned by neutron microtomography (n-µCT)[47-51] at the ANTARES Imaging facility (SR4a beamline) of the Heinz Maier-Leibnitz Center (FRM II) of Technische Universität München. The neutron beam originated from the cold source of the FRM II reactor, with an energy range mostly from 3 to 20 meV, a collimation ratio of L/D=500 (ratio between sample-detector distance and collimator aperture) and an intensity of 6.4×10^7 n/cm^2s. A 20 µm Gadox screen was used to detect neutrons. Both a cooled scientific CCD camera (Andor ikon-L) and cooled scientific CMOS camera (Andor NEO) were used as detectors. The final virtual volume of these specimens was reconstructed with an isotropic voxel size of 20.45 µm.

Data processing. Some specimens showed low contrast between the enamel and dentine in some

parts of the dataset, precluding automatic segmentation. In such cases, enamel and dentine were segmented using the magic wand tool in Avizo 8.0 (FEI Visualization Sciences Group) and manual corrections were locally applied. Use of the interpolation tool was limited to areas where the distinction between enamel and dentine could not be precisely demarcated. A volumetric reconstruction was then generated for each specimen. In most cases, the contrast resolution enabled carrying out a semi-automatic threshold-based segmentation following the half-maximum height method (HMH[52]) and the region of interest thresholding protocol (ROI-Tb[53]) taking repeated measurements on different slices of the virtual stack[54]. Because the detection of the tissue interfaces is based on attenuation at the boundary of a structure in both X-ray and neutron-based microtomography, we performed a threshold-based segmentation with manual corrections, as usually applied for X-ray acquisitions[55,56]. We quantified the degree of morphological and dimensional coherence between the X-ray microtomography (X-µCT) and n-µCT datasets of Sangiran 6a. The superimposed EDJ based on the X-µCT and n-µCT records show maximum 240 µm differences and an average of 65.7 µm variation (Supplementary Figure 19). Considering the difference in voxel size of the two original datasets (39.33 µm and 20.45 µm for the X-ray and neutron data, respectively), the differences in LM1 enamel volume (349.26 μm^3 and 346.61 μm^3), dentine-pulp volume (529.1 μm^3 and 526.7μm^3) and crown volume (878.4 μm^3 and 873.3 μm^3) are less than 1% and can be regarded as negligible.

Occlusal Fingerprint Analyses. The analysis of dental wear facets enables the reconstruction of occlusal behaviour[23]. Qualitative wear facet analysis performed by Mills[57] already led to the conclusion that in primates and insectivores the occlusal power stroke of the chewing cycle consists of two phases (buccal Phase and lingual Phase), which were later determined as Phase I and Phase II[58,59]. The chewing cycle starts with the preparatory (closing) stroke where three-body contact (tooth-food-tooth) leads to puncture-crushing activity with rare contacts of antagonistic crowns. Real chewing starts with Phase I[59], in which during stereotypic cycles tooth-tooth contacts may occur more commonly, producing guiding buccal and lingual Phase I facets through shearing activity along the buccal slopes of the buccal and lingual cusps of the lowers and complementary facets on the lingual cusp slopes of the upper molars. Phase I ends in maximum intercuspation (centric occlusion) leading into Phase II with a more or less lateral shift of the lower jaw leading to grinding activity until the last antagonistic contacts. During the recovery stroke the jaws open with no dental contacts[23,25,59]. The Phase I and Phase II pathway of the power stroke is recorded in the wear facet pattern on the occlusing molars[23,60-63]. To assess the occlusal motion pattern(s) characteristic of the Early Pleistocene robust Javanese hominid teeth considered here, we applied Occlusal Fingerprint Analysis (OFA) to attribute proportions of wear facet areas to power stroke

phases in order to compare occlusal motion patterns in a sample of extant and fossil Asian great apes and *Homo*. Occlusal macrowear areas, including wear facets following Maier and Schneck[60], were identified on virtual surface models of upper and lower molar crowns following the OFA method described in Kullmer et al.[23] and Fiorenza et al.[64]. The 3D surface data acquisition derived either from µCT datasets or from 3D surface scanning with a smartSCAN-HE (Breuckmann GmbH). Scans were taken either from originals or from high resolution casts that provide reasonable resolution of macrowear for mapping wear facet areas[61]. We used the modular software package PolyWorks® 2016 (InnovMetric Inc.) to edit the surface models. The polyline tool in the software module IMEdit was applied to interactively mark and fit closed polylines onto the model surfaces along the perimeter of wear facets in each tooth crown. By re-triangulation of the crown surfaces, the polylines became integrated into the surface models. To measure each wear facet area, triangles were selected up to each polyline curve, grouped and color-coded following the occlusal compass[23,62]. The area measurement tool in IMEdit was used to compute area in mm^2 for each wear facet. Wear facet areas were summed for chewing cycle power stroke phases[59,65]. Buccal Phase 1 (BPh I), lingual Phase 1 (LPh I) and Phase 2 (Ph II) facet area data were grouped for comparing percentage distribution of wear. To compare power stroke movements only, flat worn areas on cusp tips, identified as tip crushing areas[64], were excluded because this type of tissue loss usually results from puncture-crushing activity[59,65] and is not attributable with certainty to one of the two power stroke phases. Percentage results are illustrated in ternary plots. Each corner of the triangle represents 100% of one variable. Accordingly, a sample with an equal distribution of wear facet areas will be placed in the centre of the triangle. The plots were generated using the ggtern package v.2.2.2[66] in R v.3.4[67]. The R package RVAideMemoire 0.9-66[68] was used to perform one-way permutational multivariate analysis of variance (PERMANOVA) on the three variables (BPh I, LPh I and Ph II) separately for the maxillary and mandibular molar samples. A Bray-Curtis similarity matrix was calculated based on a 9999 permutations parameter. For both upper and lower molars the test was significant ($p<0.05$), with values for the pseudo-F model of 18.78 and 13.98 and R^2 coefficients of 0.53 and 0.57, respectively. Post-hoc PERMANOVA pairwise comparisons were run with a false discovery rate (FDR) correction (Supplementary Table 5).

3D tooth tissue proportions. Premolar and molar crowns and roots were digitally isolated at the cervix along the best-fit plane and surface rendering was performed using unconstrained smoothing for visualization, while constrained smoothing was applied for the quantitative analyses. For the molar teeth, seven linear, surface, and volumetric variables describing tooth tissue proportions were digitally measured or calculated on the molars: Ve, the volume of the enamel cap (mm^3); Vcdp; the volume of the crown dentine+pulp (mm^3); Vc, the total crown volume; SEDJ, the surface area of

the enamel-dentine junction (mm^2); Vcdp/Vc, the percent of the crown volume that is dentine and pulp (%); 3D AET (=Ve/SEDJ), the three-dimensional average enamel thickness (mm); 3D RET (=3D AET/$Vcdp^{1/3}$*100), the scale-free three-dimensional relative enamel thickness (see methodological details in refs. 24,36,69). For both premolars and molars, the following parameters were also calculated: LEA, the lateral enamel surface area (mm^2)[70]; RA, the total root surface area (mm^2)[70]; CRR (=LEA/RA*100), the crown-root ratio (%) (see Figure 4, Supplementary Figures 3-4 and Supplementary Tables 3,4,7,8). Because of the advanced degree of occlusal wear in Sangiran 6a, only crown-root proportions were assessed for the mandibular fourth premolar.

Intra- and interobserver accuracy tests of the measures run by two observers provided differences <5%. Adjusted Z-score analyses[71,72] were performed on three tooth crown tissue proportions parameters (Vcdp/Vc, 3D AET and 3D RET) for the robust Indonesian hominid maxillary (Trinil 11620, Trinil 11621 and SMF-8898) and mandibular molars (Arjuna 9, FS-77, SMF-8855, SMF-8864, SMF-8865, SMF-8879 and SMF-10055) and were compared with extant and fossil hominid samples (Supplementary Figure 20 and Supplementary Table 8). This statistical test was also applied for the CRR parameter on the maxillary molars Trinil 11620 and Trinil 11621, on the mandibular fourth premolar of Sangiran 6a and on the molars of Sangiran 6a and Arjuna 9 preserving complete roots (Figure 4, Supplementary Figure 4 and Supplementary Table 9). This statistical method allows the comparison of unbalanced samples, which is often the case when dealing with the fossil record, using the Student's t inverse distribution following the formula: [(x-m)/(s*sqrt(1+1/n)]/(Student.t.inverse(0.05;n-1)), where x is the value of the variable; m is the mean of the same variable for a comparative sample; n is the size of the comparative sample; and s is the standard deviation of the comparative sample.

Enamel thickness distribution cartographies. The 3D topographic mapping of site-specific enamel thickness variation was generated from the segmented enamel and crown dentine components of unworn to only slightly worn teeth and rendered using chromatic scales[73-77]. A rainbow chromatic scale was also used to illustrate gradual variation of enamel thickness, ranging from the thickest (in red) to the thinnest (in blue) (Figure 3).

Geometric morphometric analyses. 3D geometric morphometric (GM) analyses were conducted on the virtual surfaces of the EDJ of the maxillary molars and mandibular fourth premolar and molars. The landmarks were set along the marginal outline of the EDJ occlusal basin[77]. For the maxillary molars, six landmarks were set: three at the apex of the paracone, protocone and metacone dentine horns, and three at each intermediate lowest point between two horns along the dentine marginal ridges and oblique crest. For the lower fourth premolar, eight landmarks were

placed on the EDJ surface: four at the apex of the protoconid, metaconid, entoconid and hypoconid dentine horns and four at each intermediate lowest point between two horns along the dentine marginal ridge. For the mandibular molars, seven landmarks were placed: four at the apex of the protoconid, metaconid, entoconid and hypoconid dentine horns and three at each intermediate lowest point between two horns along the dentine marginal ridge (located by translating the cervical plane occlusally), except between the two distal horns (because of the variable presence of the hypoconulid, notably in modern humans, this cusp and the distal marginal ridge were not considered). While the specimen Trinil 11620 is virtually unworn, the protocone dentine horn apex of Trinil 11621 is affected by wear. It was thus reconstructed based on the intact height and morphology of the paracone, as well as on those of the mesial dentine horns of Trinil 11620. A similar procedure was applied to reconstruct the buccal dentine horns of Sangiran 5 and Sangiran 6a (Figure 1). We also conducted GM analyses on pulp chamber shape, setting similarly located landmarks on the cavity roof of the maxillary and mandibular molars, but not on that of the lower premolar because of a lack of expression of the distal cusps on its pulp chamber. We performed generalized Procrustes analyses, principal component analyses (PCA) and between-group principal component analyses (bgPCA) based on the Procrustes shape coordinates[78] and using genera as groups (Figures 5-6 and Supplementary Figures 9-11 and 13-15). The robust Indonesian hominid specimens were included a posteriori in the bgPCA. The analyses were performed using the package ade4 v.1.7-6[79] for R v.3.4[67]. Allometry was tested using multiple regressions[80] in which the explanatory variable is the centroid size and the dependent variables are the PC and bgPC scores. In all PCA and bgPCA, the first components only show a weak allometric signal ($0.00<R^2<0.30$), the differences between specimens thus mostly representing shape-variation. In order to statistically assess the taxonomic affinities of the robust Indonesian hominid molars, we used a supervised classification method by Support Vector Machine (SVM). Compared with linear discriminant analyses (LDA) and quadratic discriminant analyses (QDA), SVM makes no assumptions about the data, meaning it is a very flexible and powerful method[81]. SVM tests were performed on the PC scores from each GM analysis on the number of PCs needed to achieve more than 95% of the total variability (i.e., 6 to 11 PCs) (Supplementary Tables 5 and 11). Leave-2-out cross-validations were run in order to validate the model (predictive accuracy) of classification for the groups including hominins (*Homo*) on the one hand and apes (Ponginae-*Lufengpithecus*) on the other. We then tested the attribution of the Indonesian fossil hominid specimens included in the GM analyses (Arjuna 9, Sangiran 5, Sangiran 6a, FS-77, SMF-8855, SMF-8864, SMF-8865, SMF-8879, SMF-8898, SMF-10055, Trinil 11620, Trinil 11621) with respect to the model.

Data availability. The authors declare that all data supporting the findings of this study are

available within the paper [and its Supplementary information files].

References

1. Voris, H.K. Maps of Pleistocene sea levels in Southeast Asia: shorelines, river systems and time durations. *J. Biogeogr.* **27**, 1153-1167 (2000).
2. Larick, R. & Ciochon, R.L. Early hominin biogeography in island Southeast Asia. *Evol. Anthropol.* **24**, 185-213 (2015).
3. Antón, S.C., Spoor, F., Fellmann, C.D. & Swisher III, C.C. in *Handbook of Paleoanthropology* (eds Henke, W. & Tattersall, I.) 1655-1695 (Springer, New York, 2007).
4. Ciochon, R.L. in *Out of Africa I: The first hominin colonization of Eurasia* (eds Fleagle, J.G., Shea, J.J., Grine, F.E., Baden, A.L. & Leakey, R.E.) 111-126 (Springer, Dordrecht, 2010).
5. Harrison, T., Jin, C., Zhang, Y., Wang, Y. & Zhu, M. Fossil *Pongo* from the Early Pleistocene *Gigantopithecus* fauna of Chongzuo, Guangxi, southern China. *Quat. Intl.* **354**, 59-67 (2014).
6. Zhang, Y. & Harrison, T. *Gigantopithecus blacki*: a giant ape from the Pleistocene of Asia revisited. *Am. J. Phys. Anthropol*. **162**, 153-177 (2017).
7. Ciochon, R.L. The mystery ape of Pleistocene Asia. *Nature* **459**, 910-911 (2009).
8. Ibrahim, Y.K. *et al*. First discovery of Pleistocene orangutan (*Pongo* sp.) fossils in Peninsular Malaysia: Biogeographic and paleoenvironmental implications. *J. Hum. Evol.* **65**, 770-797 (2013).
9. Kaifu, Y., Aziz, F. & Baba, H. New evidence of the existence of *Pongo* in the Early/Middle Pleistocene of Java. *Geol. Res. Dev. Centre Bandung* **27**, 55-60 (2001).
10. Smith, T.M. *et al*. Taxonomic assessment of the Trinil molars using non-destructive 3D structural and development analysis. *PaleoAnthropol.* **2009**, 117-129 (2009).
11. Smith, T.M. *et al*. Disentangling isolated dental remains of Asian Pleistocene hominins and pongines. *PLoS One* **13**, e0204737 https://doi.org/10.1371/journal.pone.0204737 (2018).
12. Dubois, E. Pithecanthropus erectus*, eine menschenaehnliche Ubergangsform aus Java*. Landesdruckerei, Batavia (1894).
13. Tyler, D.E. Sangiran 5, ("*Pithecanthropus dubius*"), *Homo erectus*, "*Meganthropus*", or *Pongo*? *Hum. Evol.* **18**, 229-242 (2003).
14. von Koenigswald, G.H.R. Fossil hominids of the Lower Pleistocene of Java: Trinil. *18th Intl. Geol. Congr.* **9**, 59-61 (1950).
15. Weidenreich, F. Giant early man from Java and South China. *Anthropol. Pap. Am. Mus. Nat. Hist.* **40**,1-134 (1945).
16. Kaifu, Y. *et al*. Taxonomic affinities and evolutionary history of the Early Pleistocene Hominids of Java: Dentognathic evidence. *Am. J. Phys. Anthropol.* **128**, 709-726 (2005).
17. Kaifu, Y., Aziz, F. & Baba, H. Hominin mandibular remains from Sangiran: 1952-1986 collection. *Am. J. Phys. Anthropol.* **128**, 497-519 (2005).
18. Schwartz, J.H. & Tattersall, I. Defining the genus *Homo*. *Science* **349**, 931-932 (2015).
19. Grimaud-Hervé, D. & Widianto, H. in *Origine des Peuplements et Chronologie des Cultures Paléolithiques dans le Sud-Est Asiatique.* (eds Sémah, F., Falguères, C., Grimaud-Hervé, D. & Sémah, A.M.) 331-358 (Artcom', Paris, 2001).
20. Begun, D.R. *A Companion to Paleoanthropology*. Wiley-Blackwell, Chichester (2013).
21. Fleagle, J.G., *Primate Adaptation and Evolution, 3rd Edition*. Elsevier, London (2013).
22. Teaford, M.F. & Ungar, P.S. in *Handbook of Palaeoanthropology, 2nd Edition* (eds Henke, W. & Tattersall, I.) 1465-1494. (Springer, New York, 2015).
23. Kullmer, O., *et al*. Occlusal Fingerprint Analysis (OFA) - quantification of tooth wear pattern. *Am. J. Phys. Anthropol*. **139**, 600-605 (2009).
24. Olejniczak, A.J., *et al*. Molar enamel thickness and dentine horn height in *Gigantopithecus blacki*. *Am. J. Phys. Anthropol*. **135**, 85-91 (2008).
25. Fiorenza, L., Nguyen, N.H. & Benazzi, S. Stress distribution and molar macrowear in *Pongo pygmaeus*: A new approach through Finite Element and Occlusal Fingerprint Analyses. *Hum.*

Evol. **30**, 215-226 (2015).
26. Zanolli, C. *et al*. The Early Pleistocene deciduous hominid molar FS-72 from the Sangiran Dome of Java, Indonesia: A taxonomic reappraisal based on its comparative endostructural characterization. *Am. J. Phys. Anthropol*. **157**, 666-674 (2015).
27. Smith, T.M. *et al*. Variation in enamel thickness within the genus *Homo*. *J. Hum. Evol.* **62**, 395-411 (2012).
28. Kupczik, K., Olejniczak, A.J., Skinner, M.M & Hublin, J.J. Molar crown and root size relationship in anthropoid primates. *Front. Oral Biol.* **13**, 16-22 (2009).
29. Skinner, M.M. *et al*. Dental trait expression at the enamel-dentine junction of lower molars in extant and fossil hominoids. *J. Hum. Evol.* **54**, 173-186 (2008).
30. Schwartz, J. In *Homenaje al Dr. José Gibert Clols. Una vida dedicada a la ciencia y al conocimiento de los primeros europeos* (ed Ribot, R.) 93-110 (Publicaciones Diputación de Granada; Granada, 2016).
31. Simons, E. L. & Chopra, S. R. K. *Gigantopithecus* (Pongidae, Hominoidea) a new species from North India. *Postilla* **138**, 1-18 (1969).
32. Wang, W. New discoveries of *Gigantopithecus blacki* teeth from Chuifeng Cave in the Bubing Basin, Guangxi, south China. *J. Hum. Evol*. **57**, 229-240 (2009).
33. Koufos, G.D. & de Bonis, L. New material of *Ouranopithecus macedoniensis* from late Miocene of Macedonia (Greece) and study of its dental attrition. *Geobios* **39**, 223-243 (2006).
34. Xu, Q. & Lu, Q. Lufengpithecus lufengensis – *An Early Member of Hominidae*. Science Press, Beijing (2007).
35. Smith, T.M., *et al*. Dental ontogeny in Pliocene and Early Pleistocene hominins. *PLoS One* **10**, e0118118 doi:10.1371/journal.pone.0118118 (2015).
36. Smith, T.M. Dental development in living and fossil orangutans. *J. Hum. Evol*. **94**, 92-105 (2016).
37. Mahoney, P., Smith, T.M., Schwartz, G.T., Dean, M.C. & Kelley, J. Molar crown formation in the Late Miocene Asian hominoids, *Sivapithecus parvada* and *Sivapithecus indicus*. *J. Hum. Evol*. **53**, 61-68 (2007).
38. Schwartz, G.T., Liu, W. & Zheng, L. Preliminary investigation of dental microstructure in the Yuanmou hominoid (*Lufengpithecus hudienensis*), Yunnan Province, China. *J. Hum. Evol*. **44**, 189-202 (2003).
39. Olejniczak, A.J., *et al*. Three-dimensional molar enamel distribution and thickness in *Australopithecus* and *Paranthropus*. *Biol*. *Lett*. **4**, 406-410 (2008).
40. Noerwidi, S., Siswanto & Widianto, H. Giant primate of Java: A new *Gigantopithecus* specimen from Semedo. *Berkala Arkeologi* **36**, 141-160 (2016).
41. Bettis III, E.A., *et al*. Way out of Africa: Early Pleistocene paleoenvironments inhabited by *Homo erectus* in Sangiran, Java. *J. Hum. Evol*. **56**, 11-24 (2009).
42. Sémah, A.M., Sémah, F., Djubiantono, T. & Brasseur, B. Landscapes and hominids' environments: Changes between the Lower and the early Middle Pleistocene in Java (Indonesia). *Quat. Intl*. **223-224**, 451-454 (2010).
43. Janssen R., *et al*. Tooth enamel stable isotopes of Holocene and Pleistocene fossil fauna reveal glacial and interglacial paleoenvironments of hominins in Indonesia. *Quat. Sci. Rev*. **144**, 145-154 (2016).
44. Kelley, J. & Gao, F. Juvenile hominoid cranium from the late Miocene of southern China and hominoid diversity in Asia. *Proc. Natl. Acad. Sci. USA*. **109**, 6882–6885 (2012).
45. Ji, X-P.., *et al*. Juvenile hominoid cranium from the terminal Miocene of Yunnan, China. *Chin. Sci. Bull*. **58**, 3771-3779 (2013).
46. Nater, A. *et al*. Morphometric, behavioral, and genomic evidence for a new orangutan species. *Curr. Biol*. **27**, 1-12 (2017).
47. Kardjilov, N., *et al*. New features in cold neutron radiography and tomography. Part II: applied energy-selective neutron radiography and tomography. *Nucl. Instr. Meth. Phys. Res. A* **501**, 536-546 (2003).

48. Tremsin, A.S., *et al*. High resolution neutron imaging capabilities at BOA beamline at Paul Scherrer Institut. *Nucl. Instr. Meth. Phys. Res. A* **784**, 486-493 (2015).
49. Winkler, B. Applications of neutron radiography and neutron tomography. *Rev. Min. Geochem.* **63**, 459-471 (2006).
50. Schwarz, D., Vontobel, P., Lehmann, E.H., Meyer, C.A. & Bongartz, G. Neutron tomography of internal structures of vertebrate remains: a comparison with X-ray computed tomography. *Palaeontol. Electronica* **8** http://palaeo-electronica.org/2005_2/neutron/issue2_05.htm (2005).
51. Sutton, M.D. Tomographic techniques for the study of exceptionally preserved fossils. *Proc. R. Soc. B* **275**, 1587-1593 (2008).
52. Spoor, C.F., Zonneveld, F.W. & Macho, G.A. Linear measurements of cortical bone and dental enamel by computed tomography: applications and problems. *Am. J. Phys. Anthropol.* **91**, 469-484 (1993).
53. Fajardo, R.J., Ryan, T.M. & Kappelman, J. Assessing the accuracy of high-resolution X-ray computed tomography of primate trabecular bone by comparisons with histological sections. *Am. J. Phys. Anthropol.* **118**, 1-10 (2002).
54. Coleman, M.N. & Colbert, M.W. CT thresholding protocols for taking measurements on three-dimensional models. *Am. J. Phys. Anthropol.* **133**, 723-725 (2007).
55. Beaudet, A., *et al*. Neutron microtomography-based virtual extraction and analysis of a cercopithecoid partial cranium (STS 1039) embedded in a breccia fragment from Sterkfontein Member 4 (South Africa). *Am. J. Phys. Anthropol*. **159**, 737-745 (2016).
56. Zanolli, C., *et al*. Exploring hominin and non-hominin primate dental fossil remains with neutron microtomography. *Physics Procedia* **88**, 109-115 (2017).
57. Mills, J.R.E. Ideal dental occlusion in the primates. *Dental Practitioner* **6**, 47-63 (1955).
58. Hiiemae, K.M. & Kay, R.F. in *Craniofacial Biology of Primates, 4th International Congress of Primatology, Vol. 3* (eds Montagna, W. & Zingeser, M.R.), 28-64 (Karger, Beaverton, 1973)
59. Kay, R.F. & Hiiemae, K.M. Jaw movement and tooth use in recent and fossil primates. *Am. J. Phys. Anthropol.* **40**, 227-256 (1974).
60. Maier, W. & Schneck, G. Konstruktionsmorphologische Untersuchungen am Gebiß der hominoiden Primaten. *Zeitschrift für Morphologie und Anthropologie* **72**, 127-169 (1981).
61. Ulhaas, L., Kullmer, O. & Schrenk, F. In: *Dental Perspectives on Human Evolution: State of the Art Research in Dental Paleoanthropology* (eds Bailey, S.E. & Hublin, J.J.) 369-390. (Springer, Dordrecht, 2007).
62. Kullmer, O., Schulz, D. & Benazzi, S. An experimental approach to evaluate the correspondence between wear facet position and occlusal movements. *Anat. Rec*. **295**, 846-852 (2012).
63. von Koenigswald, W., Anders, U., Engels, S., Schultz, J.A. & Kullmer, O. Jaw movement in fossil mammals: analysis, description and visualization. *Paläontologische Zeitschrift* **87**, 141-159 (2013).
64. Fiorenza, L., *et al*. Molar macrowear reveals Neanderthal ecogeographic dietary variation. *PLoS One* **6**, e14769 http://dx.doi.org/10.1371/journal.pone.0014769 (2011).
65. Janis, C.M. in *Evolutionary Paleobiology of Behavior and Coevolution* (ed Boucot, A.J.) 241-259 (Elsevier Science, Amsterdam, 1990).
66. Hamilton, N. ggtern: An extension to 'ggplot2', for the creation of ternary diagrams. R package version 2.2.2. https://CRAN.R-project.org/package=ggtern (2017).
67. R Development Core Team. *R: A language and environment for statistical computing*. http://www.R-project.org. (2017).
68. Hervé, M. RVAideMemoire: Diverse Basic Statistical and Graphical Functions. R package version 0.9-66. https://CRAN.R-project.org/package=RVAideMemoire (2017).
69. Olejniczak, A.J. *et al*. Dental tissue proportions and enamel thickness in Neandertal and modern human molars. *J. Hum. Evol.* **55**, 12-23 (2008).
70. Kupczik, K., & Dean, M.C. Comparative observations on the tooth root morphology of *Gigantopithecus blacki*. *J. Hum. Evol.* **54**, 196-204 (2008).

71. Maureille, B., Rougier, H., Houët, F. & Vandermeersch, B. Les dents inférieures du néandertalien Regourdou 1 (site de Regourdou, commune de Montignac, Dordogne): analyses métriques et comparatives. Paleo 13, 183-200 (2001).
72. Scolan, H., Santos, F., Tillier, A.M., Maureille, B. & Quintard, A. Des nouveaux vestiges néanderthaliens à Las Pélénos (Monsempron-Libos, Lot-et-Garonne, France). Bull. Mém. Soc. Anthropol. Paris 24, 69-95 (2012).
73. Macchiarelli, R., Bondioli, L. & Mazurier, A. in: *Technique and Application in Dental Anthropology* (eds Irish, J.D. & Nelson, G.C.) 426-448 (Cambridge University Press, Cambridge, 2008).
74. Macchiarelli, R., Bayle, P., Bondioli, L., Mazurier, A. & Zanolli, C. in *Anthropological Perspectives on Tooth Morphology. Genetics, Evolution, Variation* (eds Scott, G.R., Irish, J.D.) 250-277 (Cambridge University Press, Cambridge, 2013).
75. Bayle, P., *et al*. In: *Pleistocene Databases. Acquisition, Storing, Sharing* (eds Macchiarelli, R. & Weniger, G.C.) 29-46 (Wissenschaftliche Schriften des Neanderthal Museums 4, Mettmann, 2011).
76. Zanolli, C., Bayle, P. & Macchiarelli, R. Tissue proportions and enamel thickness distribution in the early Middle Pleistocene human deciduous molars from Tighenif (Ternifine), Algeria. *C.R. Palevol* **9**, 341-348 (2010).
77. Zanolli, C. Molar crown inner structural organization in Javanese *Homo erectus*. *Am. J. Phys. Anthropol*. **156**, 148-157 (2015).
78. Mitteroecker, P. & Bookstein, F.L. Linear discrimination, ordination, and the visualization of selection gradients in modern morphometrics. *Evol. Biol.* **38**, 100-114 (2011).
79. Dray, S. & Dufour, A.B. The ade4 package: implementing the duality diagram for ecologists. *J. Stat. Softw.* **22**, 1-20 (2007).
80. Bookstein, F.L. *Morphometric Tools for Landmark Data: Geometry and Biology* (Cambridge University Press, Cambridge, 1991).
81. Gokcen, I. & Peng, J. Comparing Linear Discriminant Analysis and Support Vector Machines. In: *Advances in Information Systems: Second International Conference, ADVIS 2002* (eds Yakhno, T.) 104-113 (Springer-Verlag, Berlin, 2002).

Acknowledgements

We thank the Pusat Penelitian Arkeologi of Jakarta and the Balai Pelestarian Situs Manusia Purba of Sangiran, Java, and the French MNHN. We thank the many curators and colleagues who granted access to fossil and recent hominid materials for scanning. We are grateful to D. Grimaud-Hervé, C. Hertler, F. Sémah and H. Widianto for support. We thank J. Braga for sharing the microtomographic scans of South African fossil specimens. For scientific discussion, we thank P. Bayle, S. Benazzi, L. Bondioli, J. Braga, M.C. Dean, F. Détroit, Y. Hou, L. Mancini, B. Maureille, A. Mazurier, L. Puymerail, L. Rook, C. Tuniz, B. Wood. We would like to express our gratitude to C. Hemm, L. Hauser, M. Janocha, L. Strzelczyk for their help with the surface scanning and OFA analysis. Scanning of the Vietnamese specimens was funded by the PICS-CNRS to AMB. Research supported by the French CNRS.

Author Contributions

The study was initiated by C.Z. during his PhD research project under the supervision of R.M. Microtomographic-based data were collected and elaborated by C.Z., A.M.B., F.D., J.K., O.K., A.T.N., K.T.N., B.S., J.-J.H., M.M.S., J.X. and R.M. Quantitative data were compiled and analysed by C.Z., J.D., O.K., L.P., M.M.S and R.M. C.Z, R.M, O.K. and J.K. wrote the manuscript with contributions from all other authors.

Competing interests

The authors declare no competing interests.

Additional Information

Correspondence and requests for materials should be addressed to C.Z. (clement.zanolli@gmail.com).

643

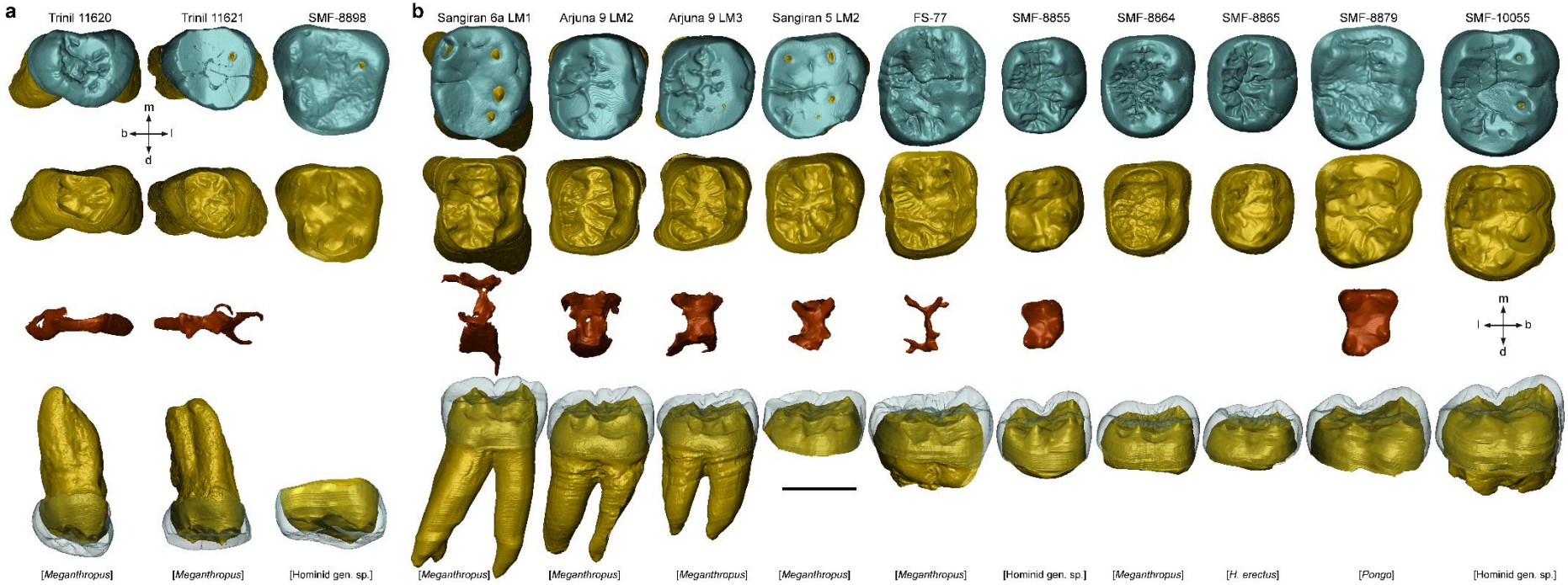

Figure 1 | Virtual rendering of the Indonesian hominid teeth examined for taxonomic reassessment. a, Maxillary molars. **b**, Mandibular molars (Supplementary Table 1). From the top, the rows show: the external occlusal morphology, the occlusal dentine, the occlusal pulp cavity and the EDJ with the overlain semi-transparent enamel cap in buccal view. For SMF-8879, only the crown is imaged. For Trinil 11621, Sangiran 5 and 6a, the worn dentine horn apices were reconstructed following the morphology of the other well-preserved cusps (see Methods). b, buccal; d, distal; l, lingual; m, mesial. Scale bar, 10 mm.

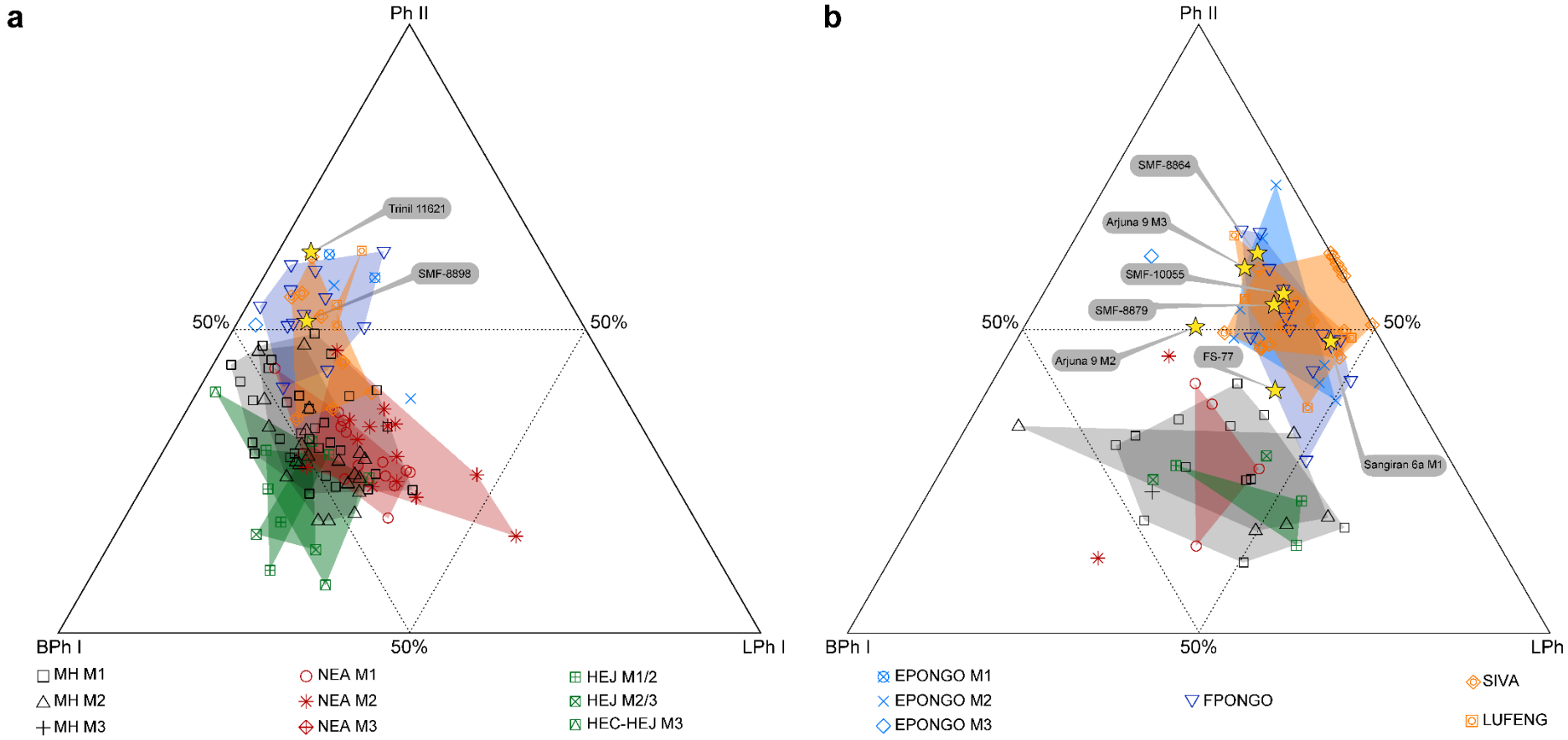

Figure 2 | Occlusal Fingerprint Analyses. **a, b**, Ternary diagram showing the proportions (in %) of relative wear areas of buccal phase I (BPh I), lingual phase I (LPh I), and phase II (Ph II) facets for the Indonesian fossil hominid maxillary (**a**) and mandibular (**b**) molars (Supplementary Table 1) compared with fossil and extant hominid specimens/samples. Each base of the triangle represents a ratio of 0% while the vertices correspond to a percentage of 100%. EPONGO, extant *Pongo*; FPONGO, fossil *Pongo*; HEC, *H. erectus* from China; HEJ, *H. erectus* from Java; LUFENG, *Lufengpithecus*; MH, modern humans; NEA, Neanderthals; SIVA, *Sivapithecus* (Supplementary Table 2).

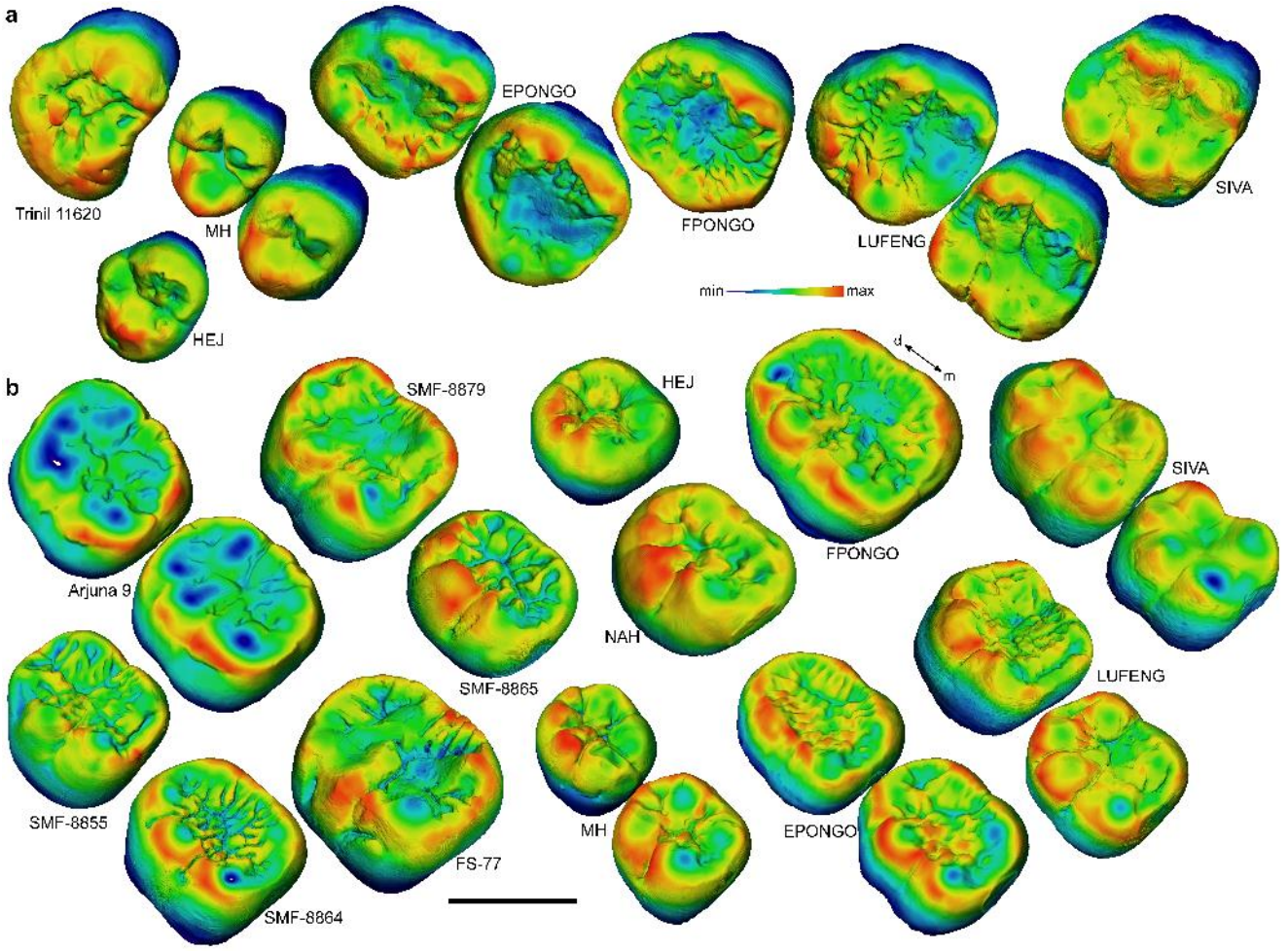

Figure 3 | Enamel thickness cartographies. a, Maxillary molars, **b**, Mandibular molars. The Indonesian hominid teeth (Supplementary Table 1) are compared with fossil and extant hominid specimens. EPONGO, extant *Pongo*; FPONGO, fossil *Pongo*; HEJ, *H. erectus* from Java; LUFENG, *Lufengpithecus*; MH, modern humans; NAH, North African late Early Pleistocene *Homo*; SIVA, *Sivapithecus* (Supplementary Table 2). Irrespective of their original side, all specimens are displayed as right antimeres in a slightly oblique occlusal perspective. Scale bar, 10 mm.

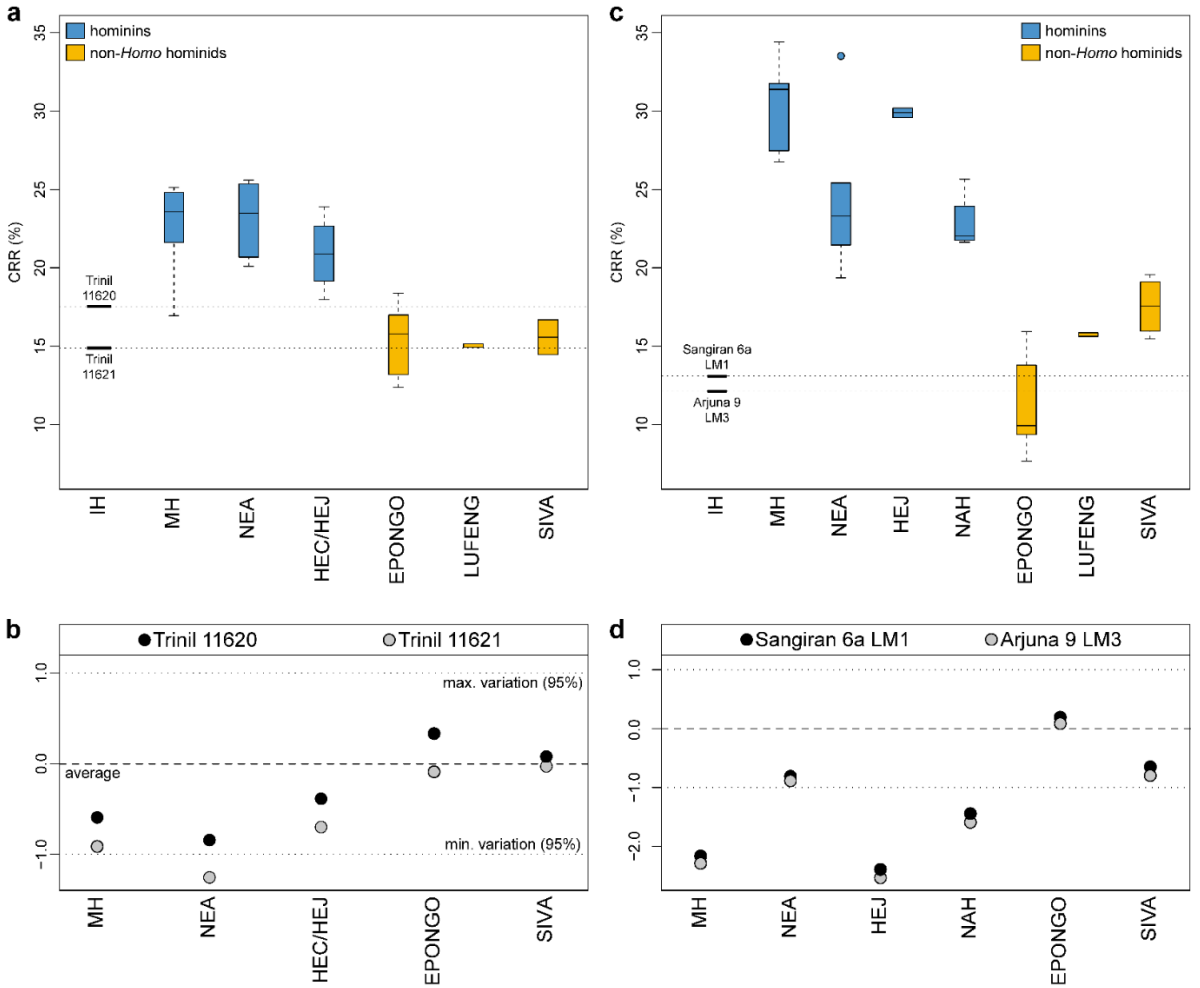

Figure 4 | Molar crown-root proportions. a, b, The crown-root ratio (CRR, in %) and its adjusted Z-score statistics for the Indonesian hominid (IH) maxillary molars from Trinil compared with fossil and extant hominid specimens/samples. **c, d**, Similar comparative analyses for the mandibular molars of Sangiran 6a and Arjuna 9 (Supplementary Table 1). The boxplots show the median, the 25th and 75th percentiles (upper and lower hinges), and the range (lower and upper whiskers). .EPONGO, extant *Pongo*; HEC, *H. erectus* from China; HEJ, *H. erectus* from Java; LUFENG, *Lufengpithecus*; MH, modern humans; NAH; North African late Early *Homo*; NEA, Neanderthals; SIVA, *Sivapithecus*

673 (Supplementary Table 2).

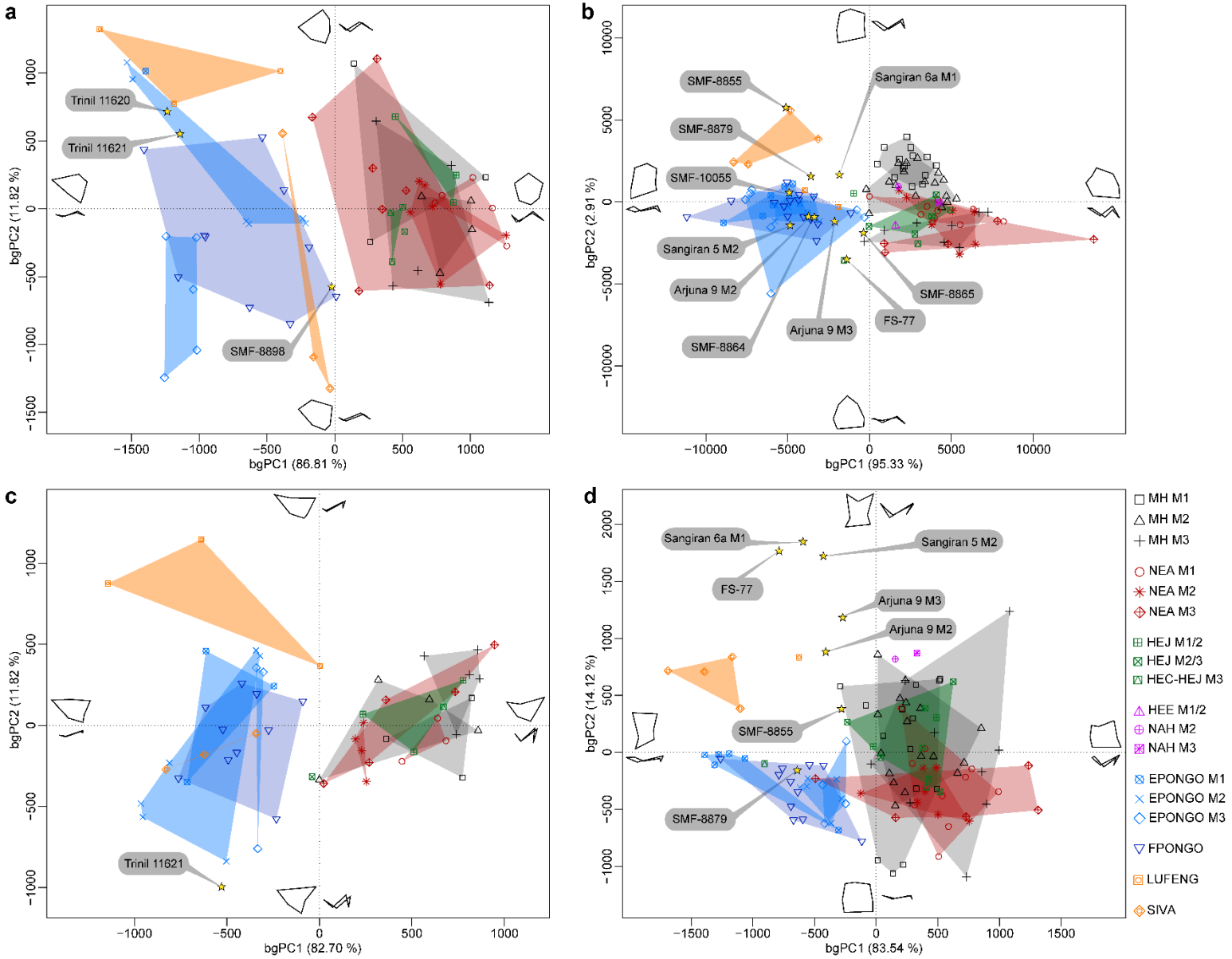
a
Trinil 11620
Trinil 11621
SMF-8898
bgPC2 (11.82 %)
bgPC1 (86.81 %)
b
SMF-8855
Sangiran 6a M1
SMF-8879
SMF-10055
Sangiran 5 M2
Arjuna 9 M2
SMF-8865
FS-77
Arjuna 9 M3
SMF-8864
bgPC2 (2.91 %)
bgPC1 (95.33 %)
c
Trinil 11621
bgPC2 (11.82 %)
bgPC1 (82.70 %)
d
Sangiran 6a M1
Sangiran 5 M2
FS-77
Arjuna 9 M3
Arjuna 9 M2
SMF-8855
SMF-8879
bgPC2 (14.12 %)
bgPC1 (83.54 %)
MH M1
MH M2
MH M3
NEA M1
NEA M2
NEA M3
HEJ M1/2
HEJ M2/3
HEC-HEJ M3
HEE M1/2
NAH M2
NAH M3
EPONGO M1
EPONGO M2
EPONGO M3
FPONGO
LUFENG
SIVA

674

Figure 5 | Geometric morphometric analyses of the EDJ and pulp chamber. a, b, Between-group principal component analyses (bgPCA) of the 3D landmarks Procrustes-registered shape coordinates of the Indonesian hominid maxillary (**a**) and mandibular (**b**) molar EDJs (Supplementary Table 1) compared with fossil and extant hominid specimens/samples. **c, d**, bgPCA of the underlying maxillary (**c**) and mandibular (**d**) pulp cavity. The wireframes at the end of the axes illustrate the extreme morphological variation trends along each bgPC in occlusal (mesial aspect upward) and buccal views (mesial aspect rightward). EPONGO, extant *Pongo*; FPONGO, fossil *Pongo*; HEC, *H. erectus* from China; HEE, *H. erectus/ergaster* from Eritrea; HEJ, *H. erectus* from Java; LUFENG, *Lufengpithecus*; MH, modern humans; NAH, North African late Early Pleistocene *Homo*; NEA, Neanderthals; SIVA, *Sivapithecus* (Supplementary Table 2).

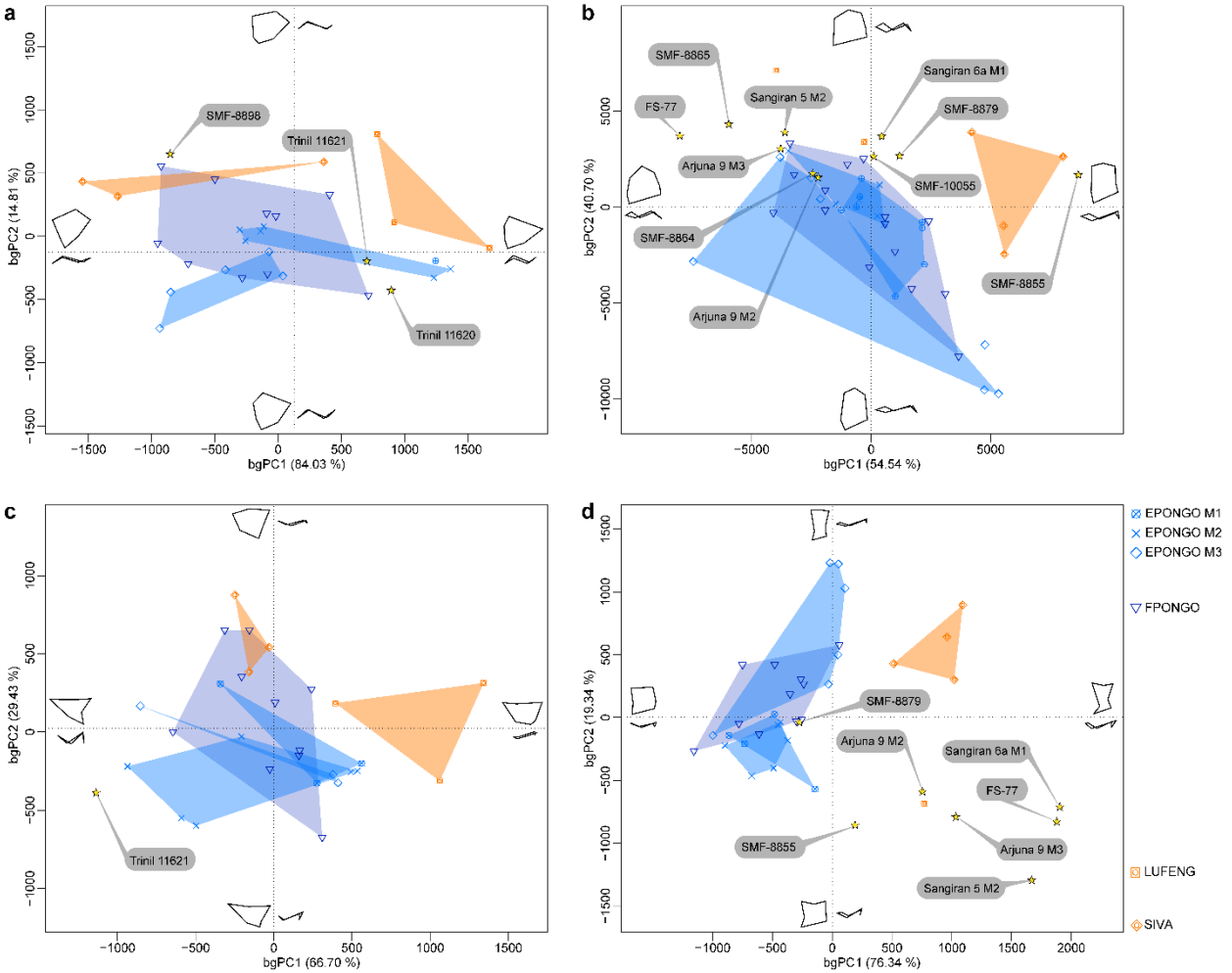

Figure 6 | Geometric morphometric analyses of the EDJ and pulp chamber in non-*Homo* hominids. a, b, Between-group principal component analyses (bgPCA) of the 3D landmarks Procrustes-registered shape coordinates of the Indonesian hominid maxillary (**a**) and mandibular (**b**) molar EDJs (Supplementary Table 1) compared with fossil and extant non-*Homo* hominid samples. **c, d**, bgPCA of the underlying maxillary (**c**) and mandibular (**d**) pulp cavity. The wireframes at the end of the axes illustrate the extreme morphological variation trends along each bgPC in occlusal (mesial aspect upward) and buccal views (mesial aspect rightward). EPONGO, extant *Pongo*; FPONGO, fossil *Pongo*;

LUFENG, *Lufengpithecus*; SIVA, *Sivapithecus* (Supplementary Table 2).